Sixth International Conference on Durability of Concrete Structures
18 - 20 July 2018
University of Leeds, Leeds, West Yorkshire, LS2 9JT, United Kingdom

Paper Number DSM01

Modelling of Capillary Pore Structure Evolution in Portland Cement Pastes Based on Irregular-Shaped Cement Particles

C. Liu, M. Zhang, G. Fang and Yun Bai
Department of Civil, Environmental and Geomatic Engineering, University College London, London, UK

Y. Zhang
School of Materials Science and Engineering, Southeast University, Nanjing, China

ABSTRACT

The pore structure plays a crucial role in durability performance of cement-based materials. However, the pore structure in cement pastes is highly dependent on the initial packing of cement particles and cement hydration process, which seems to be related to the shapes of cement particles. This paper proposed a numerical method to investigate the effect of cement particle shapes on capillary pore structures in cement pastes. In this study, irregular-shaped cement particles with various shapes are generated using a novel central growth model, and then incorporated into CEMHYD3D model to simulate Portland cement hydration. Some home-made programs of determining pore structure parameters including porosity, pore size distribution, connectivity and tortuosity are subsequently performed on the extracted three-dimensional network of capillary pore structure in cement pastes. The modelling results indicate that shape-induced large surface area in more non-equiaxed irregular-shaped cement particles can improve pore structure parameters in hardened cement pastes, but this effect will be slight in the later curing period and at a low water-to-cement ratio. In addition, the less considered geometric difference plays a role in pore structure evolution especially for extremely non-equiaxed cement particle. However, the geometric attribute has a weak effect on pore structure parameters overall. The modelling results can provide a new insight into durability design in cement-based materials by means of manipulating cement particle shape in the future.

Keywords: modelling; cement particle shape; irregular shapes; hydration; capillary pore; microstructure.

1.0 INTRODUCTION

The network of pore structure of cement paste is crucial to mass transport properties in cement-based materials, which is usually considered as indicators to assess the durability and predict the service life of reinforced concrete structures (Liu *et al*., 2016). Different from traditional porous materials consisting of agglomerated particles, e.g., ceramics and metals, the topology of pore structure in cement-based materials is much more complicated due to the multi-scale nature of microstructure and evolution of microstructure as a result of continuous hydration of cement. Pores in cement-based materials can be mainly classified into capillary pores and gel pores without a fixed critical threshold (Huang *et al*., 2015; Mindess *et al*., 2003). As cement hydration proceeds, pore space between cement particles is gradually filled by hydration products, which leads to a refinement of capillary pore structure. By contrast, the increasing C-S-H containing gel pores can result in the formation of gel pore structure with its comparatively stable intrinsic attribute of structure (Kuo *et al*., 2006). Compared to small and tortuous gel pores, changeable capillary pore structure plays a decisive role in transport properties in cement-based materials. Therefore, understanding the nature of capillary pore structure is of significance for investigating durability performance in cement-based materials.

It has been proved that pore structures in sintering porous materials, e.g., pore size distribution and pore tortuosity are strongly governed by performance of starting powders (Ishizaki *et al*., 2013). Particle shape, which is an important fact to be considered in starting powder, strongly influences properties of porous materials. In terms of cement-based materials, the evolution of capillary pore structure is highly dependent on cement hydration process and microstructural development. Many authors have focused on the experimental investigation of effects of raw material performance on pore structures in hardened cement pastes (Chindaprasirt *et al*., 2005; Chindaprasirt *et al*., 2007; Tsivilis *et al*., 1999). Although numerous studies concentrated on the effects of fineness (surface area) and chemo-activity of raw materials, to the authors' best knowledge, that of particle shapes on pore structures has not been yet fully explored. This is attributed to that there is no effective technique for manipulating shapes of

cement particles during production process in cement industry until now. In addition, the properties of cement powder, e.g., specific surface area and particle shape, are interacted during grinding process, which is impossible to isolate the effects of specific variables in experimental investigation. Fortunately, numerical simulation may provide an alternative way to investigate the particle shaped effects on capillary pore structures in hardened cement pastes.

This study aims at understanding the detailed relationship between cement particle shapes and pore structures in hardened cement pastes based on previously proposed cement hydration model using irregular-shaped particles. Firstly, the 3D microstructures of cement pastes are simulated using CEMHYD3D model based on different irregular-shaped cement particles generated using central growth model. The mechanism of central growth model is simply reviewed and detailed simulated cases are described in this section. Subsequently, some numerical methods for determining 3D pore structure parameters including porosity, pore size distribution, pore connectivity and pore tortuosity along with home-made programs are detailed described. Finally, the obtained pore structure parameters in cement pastes consisting of different shaped cement particles are analysed and compared to each other at water-to-cement ratios of 0.3, 0.4 and 0.5 with and without considering cement hydration kinetics.

2.0 MODELLING AND SIMULATION

2.1 Modelling of Microstructural Development

Figure 1. Shows a flow chart of the generation of microstructure of irregular-shaped cement using the proposed central growth model. The entire procedure can be divided into five steps. Step I and II are related to the generation of individual cement particles, while Step III to V are associated with random packing of these particles.

Step I: Initially, a 3D discrete box with the same resolution as that of RVE is constructed and used as growing space, which should be large enough to accommodate single particle. Subsequently, the coordinates of the central point in this discrete growing space and a set of default eigenvectors for growing irregular-shaped particles are transferred into a list. The values (0-100) of the eigenvector in each square (or cube) represent the growing probabilities of the particle in the corresponding dimension.

Step II: Firstly, the coordinates of the first node in the list (i.e., central point) are read and the corresponding pixel is turned into a blue particle pixel. Its eight neighbouring pixels highlighted in yellow colour are then activated and a set of eight probability values between 0 and 100 are generated for them sequentially based on a Monte Carlo simulation. The eight probability values are then compared with the corresponding characteristic values of the special irregular particles, respectively. If the pointed cell has a probability value smaller than its corresponding characteristic one, the cell would be turned into a part of the particle. There steps are repeated on the activated neighbouring pixels until the target area of this particle is achieved.

Step III: Due to the similar orientation of particles produced by the same eigenvector, the grown cement particle needs to be rotated by a random angle α in the growing space to keep its random orientation in the RVE.

Step IV: Boolean operations are used to eliminate “sieve holes” after rotations.

Step V: Once the individual particle with a random orientation is reconstructed in the growing space, the next step is to throw this particle into RVE of cement mixes. Fig. 2 shows the packing structure of pre-hydrated cement pastes consisting of different shaped cement particles.

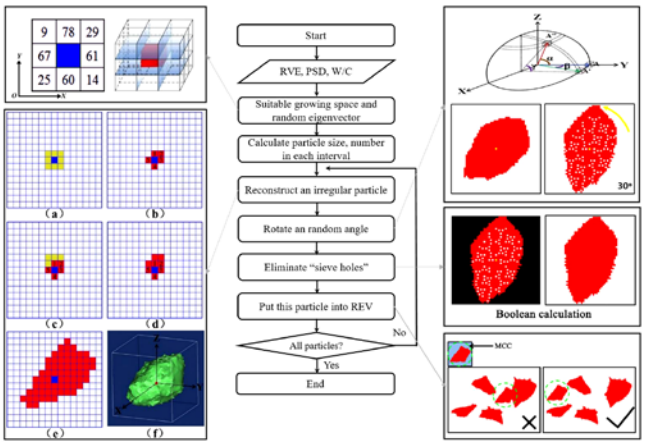

Fig. 1. Flow chart for the generation of an irregular-shaped particle and particle packing

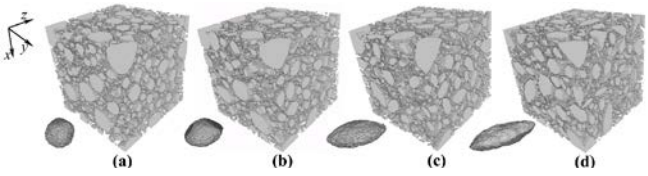

Fig. 2. Schematic of pre-hydrated microstructures generated using (a) spherical, (b) flat-, (c) intermediate- and (d) elongated-shaped cement particles at the w/c ratio of 0.4

The pre-hydrated cement pastes consisting of four representative shaped cement particles are respectively incorporated into CEMHYD3D model (Bentz, 1995; Bentz, 1997) to simulate hydration

process. Cement hydration processes of water-to-cement (w/c) ratios of 0.3, 0.4 and 0.5 are simulated and determined. Four representative shapes are named spherical, flat, intermediate and elongated shapes, as shown in Fig. 2. In CEMHYD3D model, modelling hydration is carried out via cycles of dissolution, diffusion and reaction according to known reaction equations of mineral phases. The relationship between computational cycle (n) and real time (t) is satisfied with equation of parabolic hydration kinetics

$$t = \beta n^2 \tag{1}$$

where β is the conversion factor. In terms of curing conditions, the curing temperature is constant at 20 °C for all cement pastes with a saturated condition. With respect input parameters of real cement, a Chinese Portland cement named P.I cement (similar to the ASTM Type I Portland cement) with mineral phases of 52.36% C_3S, 29.75% C_2S, 4.77% C_3A and 13.12% C_4AF respectively is used. The above described procedure of modelling cement hydration with irregular-shaped cement particles can refer to our recent publication (Liu *et al*., 2018a).

2.2 Modelling of parameters of pore structure

Porosity

In the 3D voxel-based microstructure, pore and solid phase can be labelled respectively and pore structure should also be extracted from the microstructure. The pore voxel can be determined by point-to-point scanning. Porosity (P) is obtained following the equation

$$P = \frac{V_p}{V_b} \tag{2}$$

where V_p and V_b are pore volume and bulk volume of the cement paste respectively.

Pore size distribution

A discrete PSD named 3D voxel-erosion method (Zhang *et al*., 2017) alongside a home-made program is proposed to achieve PSDs in microstructures generated using different shaped particles. In this method shown in Fig. 3, voxels in each 2D section are firstly labelled to be solid and capillary pore phase based on their occupancy. Subsequently, pore voxels sharing at least one face with a solid voxel are marked with number 1. In the next step, pore voxels sharing at least one face with the voxels labelled 1 are labelled 2. The same process is iterated until all pore voxels are marked with the number of steps required to erode them from the pore-solid boundaries. The maximum number of steps in each isolated pore in 2D is the radius of this pore in voxel-unit. This algorithm is successively employed on each 2D section. Finally, combined with the resolution in the digital structure, PSD can be determined. Although voxel-erosion method is one of many possible definitions of pore size and ignores the information regarding pore-topology, e.g., connected and disconnected pores, it can quickly get relative results of PSDs in discrete cement paste microstructures.

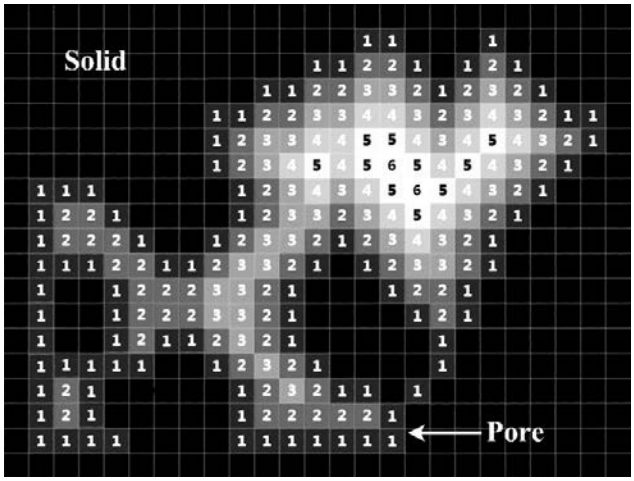

Fig. 3. Definition of pore size. Solid phase is black pixels and pores are grey pixels marked with numbers denoting the step number required to erode from the closest solid phase pixel

Pore connectivity

To quantitatively characterize capillary pore depercolation process in microstructural evolution, the well-known “burning algorithm” (Bentz and Garboczi, 1991; Gao *et al*., 2013) is employed. In the voxel-based microstructure, the first pore voxel of surface slice in RVE chosen as burning point is burnt; the pore voxels contacting this burning point are accordingly burnt, by that analogy, until all connected pore voxels in this pore cluster containing the first burning point are burnt. If two pore voxels contact by face-to-face form in 3D, these two pore voxels are connected, while two pore voxels contact by other two forms, edge-to-edge and point-to-point form, these two are disconnected. If the pore voxels can be burnt from one surface to the opposite surface, this pore cluster is connected. In order to model cement hydration in infinite field, periodic boundary conditions are employed in this RVE. As a result, connectivity in boundary surfaces should also be considered. In this study, only pore clusters with connected pores in two surface slices are determined to be connected. Following this process, all connected pore clusters can be detected, e.g., pores of labelled 1 and 2 in Fig. 4.

Pore tortuosity

To quantitatively determine pore tortuosity in hardened cement pastes, numerical simulation should be implemented on 3D microstructures. In this work, a 3D random walk simulation (Dong *et al*., 2017; Promentilla *et al*., 2016; Promentilla *et al*., 2009) of simulating self-diffusion behavior along with

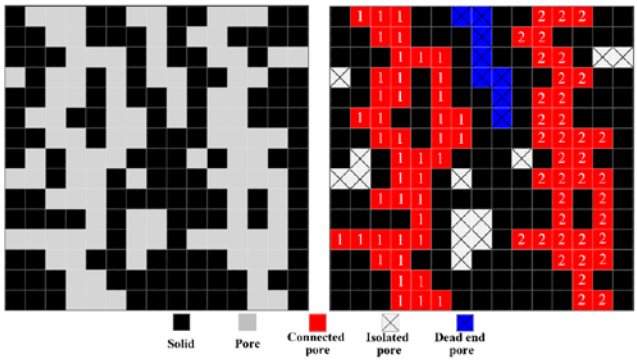

Fig. 4. Schematic illustration of pore types and burning algorithm

a home-made program is employed to compute tortuosity by the mean square displacement (MSD) of randomly walking "ants" in the percolating capillary pore voxels as a function of time. The programming mechanism is as follows: sufficient "ants" used to model diffusion specimen in pore structure migrate on the pore voxel selected randomly, as the start position of the lattice walk trial at integer time equals to 0. A trial move is performed with the space step of one voxel distance in one of the six possible directions. The ant then executes a random jump to one of the nearest pore voxels and the time of walk is incremented by one unit integer time after the jump. If the randomly chosen voxel is a non-pore phase, the ant will stay at previous location and the jump is not performed, while the time is still incremented by one unit. As time elapses, the ants will go out of the discrete RVE. This out-leaching phenomenon is undesirable and inevitable because of limited system size. As such, periodic boundary conditions on the 3D microstructures are employed to address this out-leaching problem, which is in accordance with previous performance. After an abundant number of walking steps (t) of sufficient ants (n), the diffusion tortuosity can be determined by the following equation:

$$\tau_D = \frac{\left\langle l_f^2(t)\right\rangle}{\left\langle l_{cp}^2(t)\right\rangle} \quad \text{as } t \to \infty \tag{3}$$

where $\left\langle l_f^2(t)\right\rangle$ and $\left\langle l_{cp}^2(t)\right\rangle$ are mean square displacement in free space and porous media respectively. The mean square displacement is satisfied with

$$\left\langle l^2(t)\right\rangle = \frac{1}{n}\sum_{i=1}^{n}\begin{bmatrix}\left(x_i(t)-x_i(0)\right)^2-\left(y_i(t)-y_i(0)\right)^2\\-\left(z_i(t)-z_i(0)\right)^2\end{bmatrix} \tag{4}$$

where $x_i(t)$, $y_i(t)$ and $z_i(t)$ are the coordinate of ant i at time t, and $x_i(0)$, $y_i(0)$ and $z_i(0)$ are the starting position of ant i. The detailed algorithm for determining parameters of capillary pore structures can refer to our recent publication (Liu *et al*., 2018b).

3.0 RESULTS AND DISCUSSION

3.1 Porosity

The evolution of capillary porosities in simulated hardened cement pastes consisting of different shaped cement particles is illustrated in Fig. 5. In all cement pastes regardless of particle shapes and w/c ratios, porosity evolutions show the similar changing tendency with time elapsing. In detail, porosities in cement pastes at the same w/c ratio decrease slightly in the early 10 h, then fall dramatically in the next 100 h, accounting for over 40% of initial porosities, finally reach a steady tendency after 100 h. In terms of the effect of the shaped discrepancy, cement pastes with elongated-shaped particles show the greatest decreasing tendency especially between 10 h and 100 h compared to other ones. At w/c ratios of 0.4 and 0.5, cement pastes consisting of elongated- and intermediate-shaped particles contain less capillary pores compared to that of spherical and flat-shaped particles. It means that the more non-equiaxed cement particle is, the much greater decrease of porosity it will have. It can be attributed to surface area difference in essence where cement particle with less equiaxed has larger surface area. Cement particles with large surface area can dramatically improve hydration rate in the early curing period.

However, the difference of porosity is disappeared in later curing period and at a low w/c ratio, e.g., cement pastes after curing time of 100 h at the w/c ratio of 0.3. This is ascribed to that water content at w/c=0.3 is not sufficient for cement to totally hydrate. Although cement consisting of spherical and flat-shaped particles is with low hydration rate, its hydration potential is the same as that consisting of high surface area particles. When the hydration rate of cement with high surface area is decreasing even stopped in the later period, one with low surface area can still hydrate due to the remaining considerable water content. It should be noticed that cement pastes made up of spherical particles shows the similar changing curve of porosity as that made up of flat-shaped particles in spite of with different shapes. This is attributed to that simulated discrete spherical shape with many local small protuberances in this study is not the perfect digitalized sphericity, which increases surface area of spherical particle. This leads to slight surface area difference between pre-hydration microstructure consisting of spherical and flat-shaped cement particles. As such, hydration kinetics affected by surface area in these two cement pastes show great similarity.

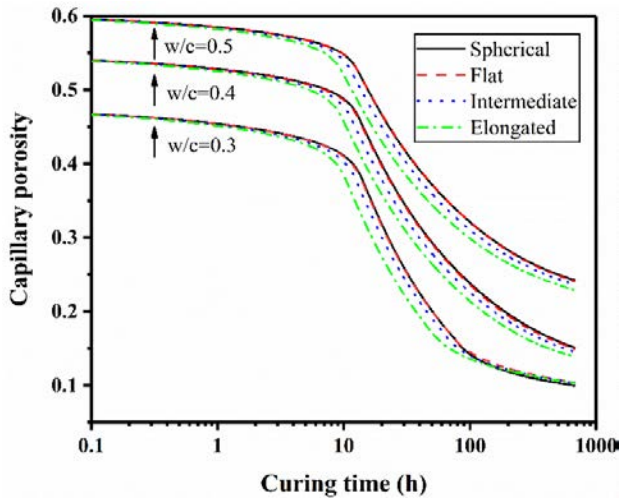

Fig. 5. Porosity in simulated cement pastes consisting of different shaped cement particles

3.2 Pore Size Distribution

The program of 3D voxel-erosion method is performed on the networks extracted from simulated cement pastes microstructures at curing time of 0, 1, 7 and 28 d respectively. As shown in Fig. 6, the representative pore network extractions consisting of spherical and elongated-shaped cement particles at the w/c ratio of 0.4 are visualized. It can be found that initial pore clusters become smaller and some pore voxels extend to the locations where solid phase voxels occupy previously as cement hydration proceeds. Fig. 7 shows the effect of particle shapes on pore size distributions in cement pastes with different curing time at w/c=0.3, 0.4 and 0.5. It can be found that with cement hydration from 0 d to 28 d, pore sizes in cement pastes gradually decrease due to the fill of hydration products in capillary pores. Additionally, in accordance with the effect of particle shapes on porosity, the less equiaxed particles with higher surface area can lead to lower pore size in the hardened cement paste at early curing age, e.g., 1 d, because of higher hydration rate. However, this shaped effect on pore size will be decreasing after curing time of 1 d. The reason is that the effect of higher surface area resulting from initial particle shape will gradually retard with cement hydration, especially for the particle of less shaped difference, e.g., flat- and intermediate-shaped particles. In respect to the effect of the w/c ratio, the increasing w/c ratio can extend shaped effect on pore size in cement pastes, as shown in Fig. 7(c). At curing age of 1 d, the middle pore size in cement paste consisting of elongated-shaped particles at w/c=0.5 with around 7.5 μm is even only 0.5 time of that consisting of spherical particles. However, this difference of middle pore size is very slight for the same shaped cement pastes at w/c=0.3. Consequently, irregular-shaped particles with high surface area is beneficial to decreasing pore size in cement pastes, especially at a high w/c ratio.

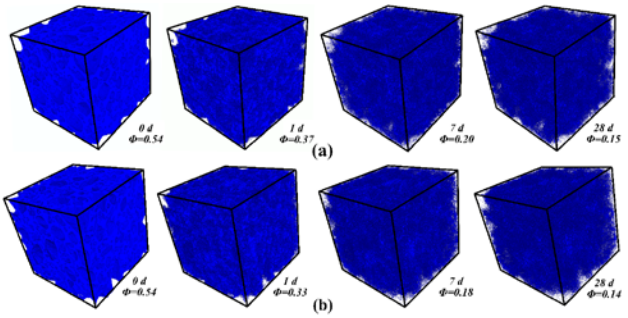

Fig. 6. 3D pore structures of hardened cement pastes at curing time of 0, 1, 7 and 28 d with the w/c ratio of 0.4.(a) spherical particles. (b) elongated-shaped particles. Φ means capillary porosity

shaped particles also has influence on cement hydration process. As a result, in order to eliminate kinetics in cement hydration process, the program for determining pore size distribution is also carried out on the networks at degree of hydrations (DoHs) of 0, 0.2, 0.4, 0.6 and 0.8. Figure 8 shows the effect of particle shapes on pore size distribution with different degree of hydrations at w/c ratios of 0.3, 0.4 and 0.5. As can be seen from Fig. 8(a-c), particle shaped difference has great influence on pore size at early curing time for a high w/c ratio (0.5). For example, middle pore size in hardened cement pastes with the w/c ratio of 0.5 at DoH of 0.2 consisting of elongated-shaped particles is almost 2.0 μm which is much smaller than that consisting of spherical ones with around 8.0 μm at the same conditions. Nevertheless, this effect can be neglected for capillary pores in hardened cement pastes at high DoHs (0.6 and 0.8) for small w/c ratios (0.3 and 0.4). This can be ascribed to that non-equiaxed particles are beneficial to decreasing particle-to-particle spacing in packing system compared to equiaxed particles, e.g., spherical shape (Xu and Chen, 2012). At the low DoH, the packing effect of initial non-equiaxed cement particles with local sharp surface regions are crucial to decreasing capillary pore size. However, the surficial shape of initial cement particle for non-equiaxed particle is gradually ambiguous and tends to be more spherical with cement hydration (Bullard and Garboczi, 2006). In addition, the geometry of hydration products as filled solids of capillary pores shows great disorder and randomness in the simulated hardened cement pastes. The geometric effect of cement particles becomes more and more ignorable at the high DoH. As such, geometric effect of cement particles has effect on pore size in cement pastes in the early period, while this effect will be slight for cement pastes with low w/c ratios and high DoH.

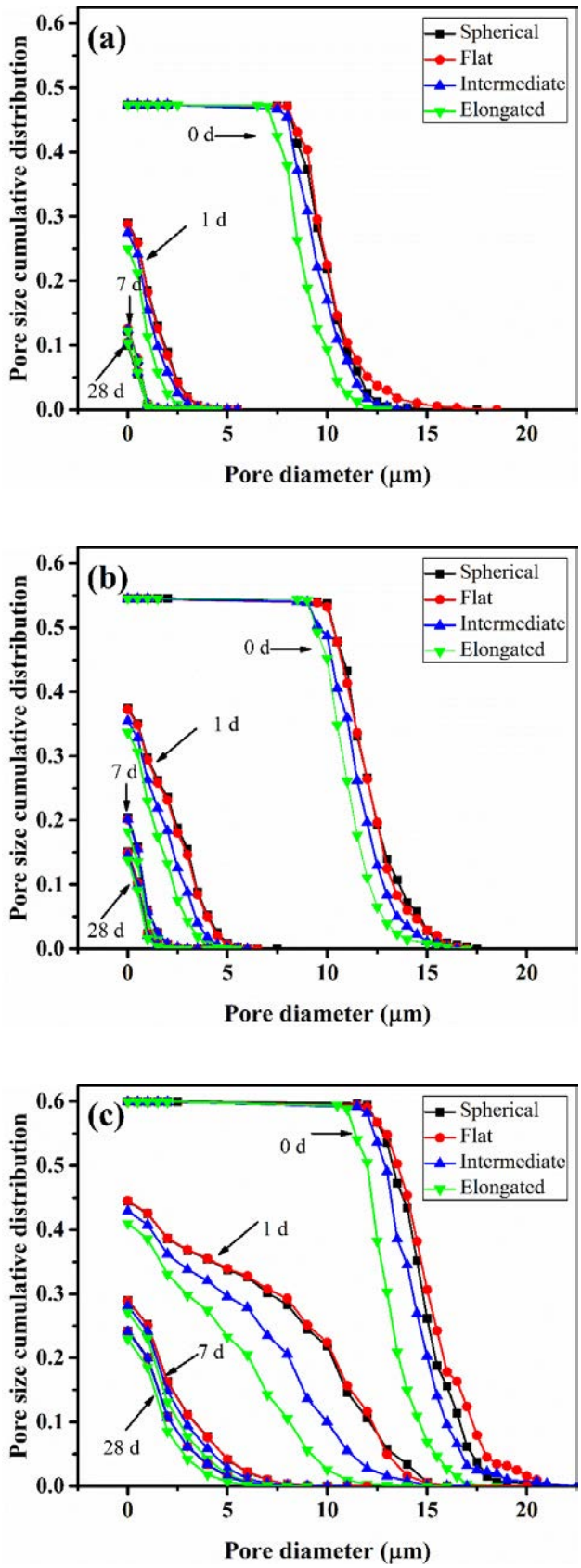

Fig. 7. Pore size distributions in simulated cement pastes with different curing time at w/c ratios of (a) 0.3 (b) 0.4 and (c) 0.5

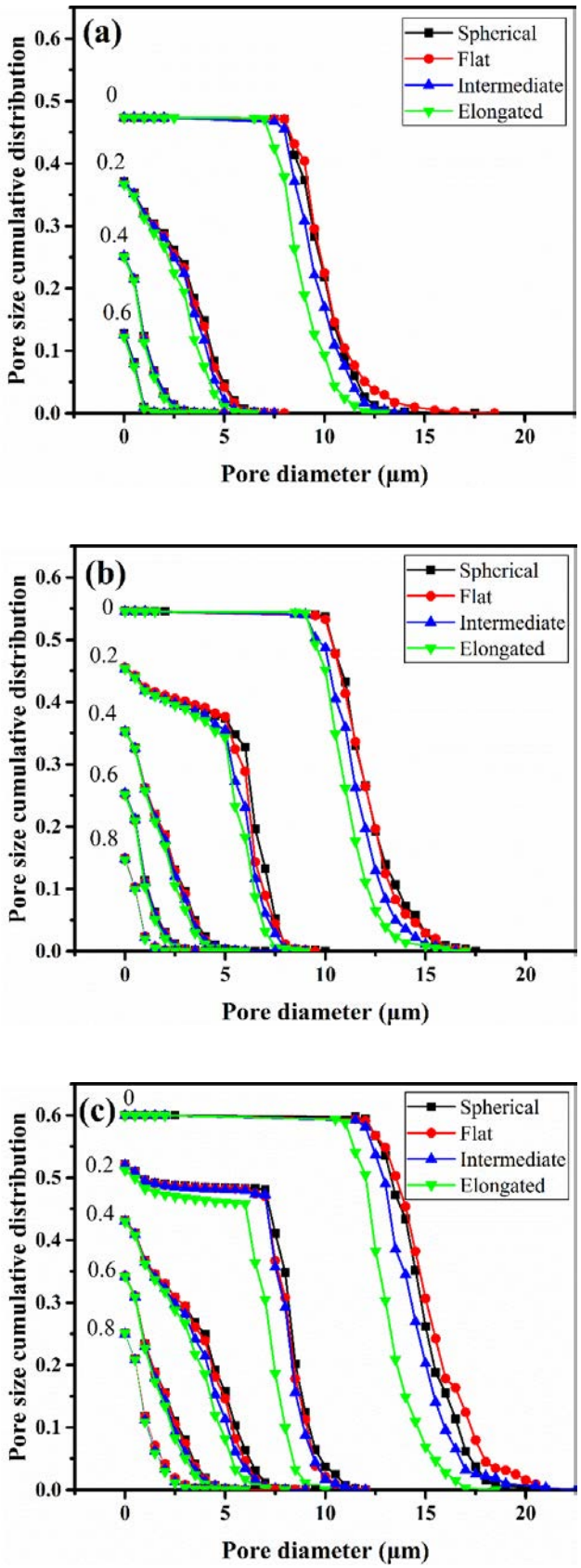

Fig. 8. Pore size distributions in hardened cement pastes with different degree of hydrations (0, 0.2, 0.4 0.6 and 0.8) at w/c ratios of (a) 0.3 (b) 0.4 and (c) 0.5

3.3 Pore Connectivity

Figure 9 illustrates the continuous evolution of connectivity of capillary pore in cement pastes at w/c ratios of 0.3, 0.4 and 0.5 as time elapses. It can be seen that cement pastes at the w/cs of 0.3 and 0.4 can reach depercolation of capillary pore, while that at the w/c of 0.5 cannot. Moreover, the time of reaching depercolation at various w/cs is dramatically different. For example, the time of reaching depercolation in cement pastes at w/c=0.3 is several dozens of hours, by contrast, the depercolated time at w/c=0.4 is even a few hundreds of hours with one order of magnitude difference. In addition, from the tendency of curves of different shaped particles at the same w/c, the less equiaxed particles is positive to the connectivity of capillary pore. The time of reaching depercolation in cement pastes comprised of different shaped particles at the same w/c is various, but the difference of time is decreasing as w/c ratio decreases. For example, the time of depercolation in cement pastes made up of elongated-shaped particles at w/c=0.4 occurs at around 220 h, but this time occurs at 520 h for spherical particles, 300 h difference. However, this difference is retarded for w/c=0.3 with only 30 h.

To vividly visualize the depercolated process of capillary pores, the case of extracted pore networks in cement pastes consisting of spherical and elongated-shaped particles in accordance with that in Fig. 6 is shown in Fig. 10. Red voxels and blue voxels are connected and disconnected pores. It can be intuitively found that elongated-shaped particles can accelerate depercolation of capillary pore compared to spherical particles.

Figure 11 shows the evolution of connectivity of capillary pores with DoH. It can be found that particle shapes have influence on the connectivity of capillary pores in hardened cement pastes. The less equiaxed cement particles are positive to depercolation of capillary pores, but this geometric effect of particle shapes is pretty slight. To directly correlate with capillary porosity, the evolution of connectivity of capillary pore is shown in Fig. 12. In Fig. 12, although the changing tendency of connectivity of capillary pore with porosity is different at low DoH due to the porosity difference and early local discrepancy of pore structure in 3D microstructure, the gradually same tendency will yet occur at a low porosity of around 0.25. Furthermore, the depercolated porosity of elongated-shaped particles at the same w/c is slightly superior to that of other shaped particles, which implies that the less equiaxed particles is beneficial to decreasing connectivity of capillary pores. In terms of depercolated capillary porosity, the values of all cement pastes are between 0.16 and 0.18 which are slightly smaller than inherent depercolation porosity of around 0.15 in CEMHYD3D model using digitalized spherical particles at resolution of 0.5 μm/voxel. These all demonstrates that geometric effect of cement particles plays a weak role in depercolation process of capillary pores in cement pastes, while pore-to-solid ratio (porosity) is still the most pronounced influence factor to determine depercolation process.

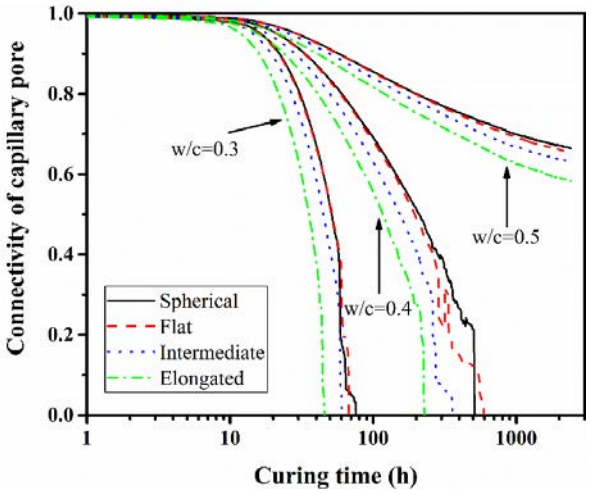

Fig. 9. Evolution of connectivity of capillary pore in simulated cement pastes against curing time.

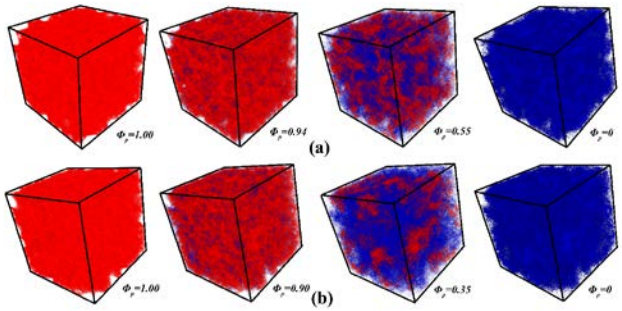

Fig. 10. 3D percolated (red) and depercolated pore structures (blue) in hardened cement pastes consisting of (a) spherical and (b) elongated-shaped particles at curing time of 0, 1, 7 and 28 d. Φ_p means percolated capillary porosity

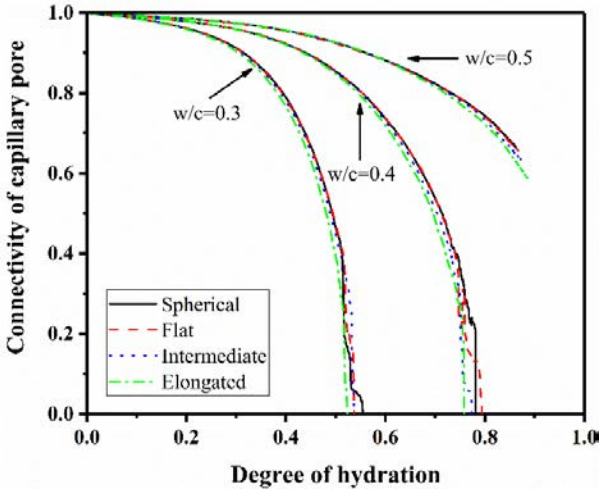

Fig. 11. Connectivity of capillary pore against degree of hydration

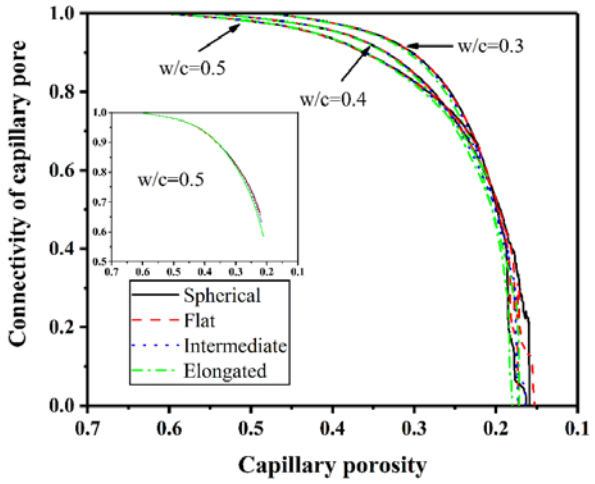

Fig. 12. Connectivity of capillary pore against capillary porosity.

3.4 Pore Tortuosity

In order to achieve diffusion tortuosity of pore network in cement pastes, the program of random walk algorithm is implemented on these pore structures at the same curing time and degree of hydration, respectively. Mean square displacements in pore structures at curing time of 0, 1, 7 and 28 d for different shaped particles against time of lattice walk are illustrated in Fig. 13. It can be seen that as cement hydration proceeds, the slope of curve of mean square displacement against time of lattice of walk is decreasing, which means pore structures are becoming more tortuous. In Fig. 9, it can be concluded that capillary pores in cement pastes at curing age of 7 d and 28 d for w/c=0.3 and at curing age of 28 d for w/c=0.4 are disconnected. Therefore, the diffusion tortuosity of capillary pores is infinite in the corresponding simulated cement paste, which means mass transport properties are manipulated by porous C-S-H in this state (Garboczi and Bentz, 1992; Zhang *et al*., 2017). In addition, the difference of pore tortuosities in the initial packing microstructures is slight in spite of with the shaped discrepancy, which is in agreement with the finding that sand shaped effect has a weak influence on diffusivities in mortars consisting of various shaped aggregates (Abyaneh *et al*., 2013). Nevertheless, the shape-induced difference of pore tortuosity becomes much larger with cement hydration. The cement pastes made up of less equiaxed particles have larger pore tortuosity. With respect to the w/c ratio, cement pastes with a higher w/c ratio shows lower pore tortuosity. Based on Eq. (3), Fig. 14 illustrates the detailed values of pore tortuosity. It can be found that the cement pastes at a low w/c are more tortuous than that at a high w/c at the same curing age. It is also surprising to find that the values of pore tortuosity in the same microstructural process may even have two orders of magnitude difference, e.g., the microstructure at w/c=0.4 with values of tortuosity of around 1.5 at 0 d and around 200 at 7d shown in Fig 14 (b). This demonstrates

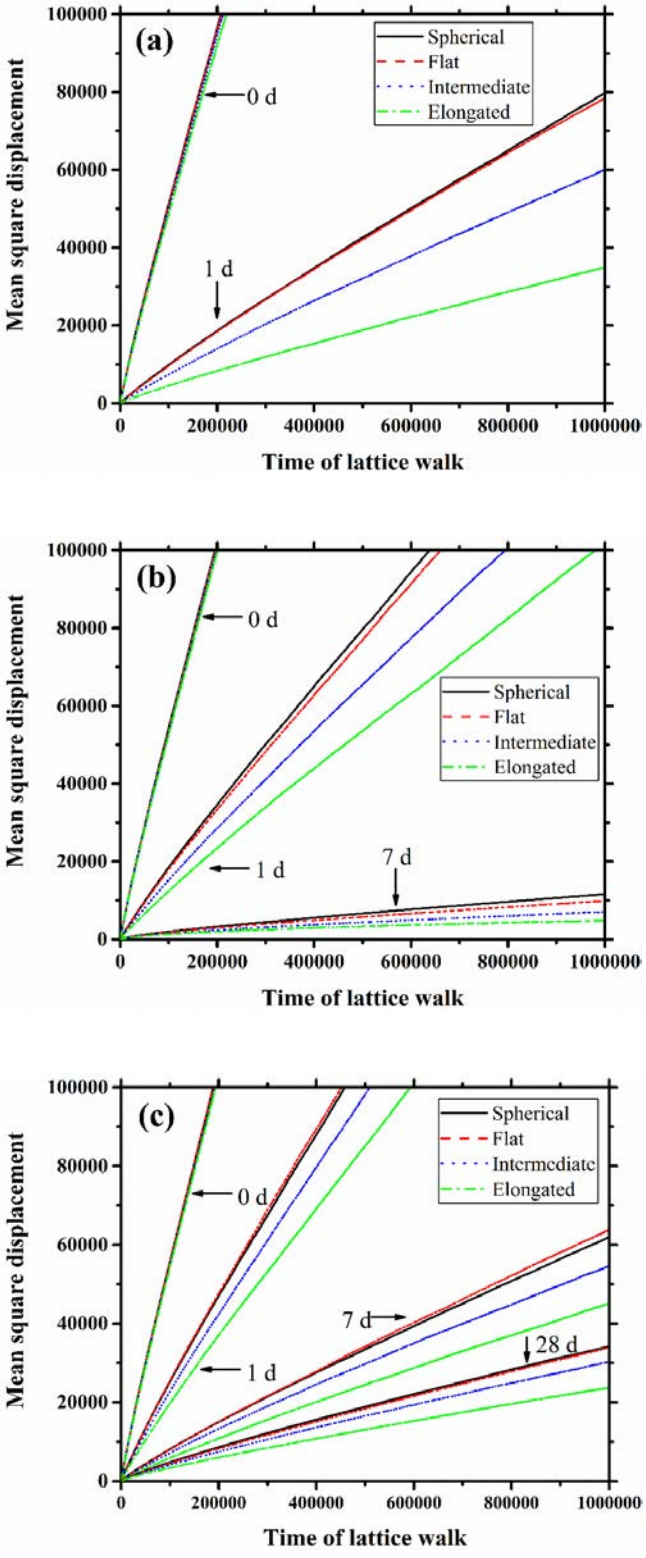

Fig. 13. Mean square displacement against time of lattice walk at w/c=0.3 (a), 0.4 (b) and 0.5 (c).

that cement hydration process plays a decisive role in decreasing transport properties in cement pastes compared to cement particle packing.

Figure 15 shows the detailed values of pore tortuosity in 3D pore network at DoHs of 0, 0.2, 0.4, 0.6 and 0.8 for different shaped particles.

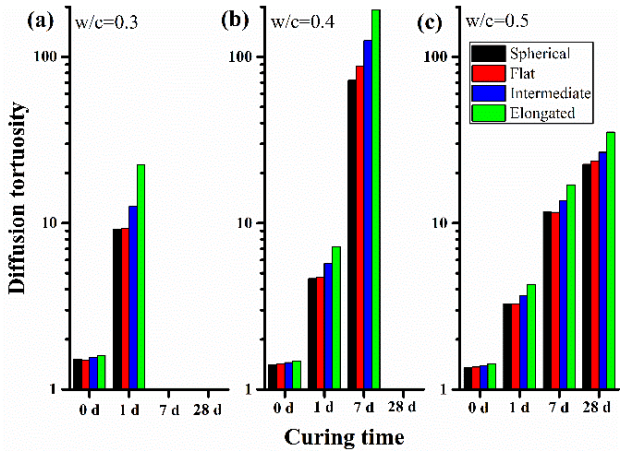

Fig. 14. Diffusion tortuosity in hardened cement pastes against curing time.

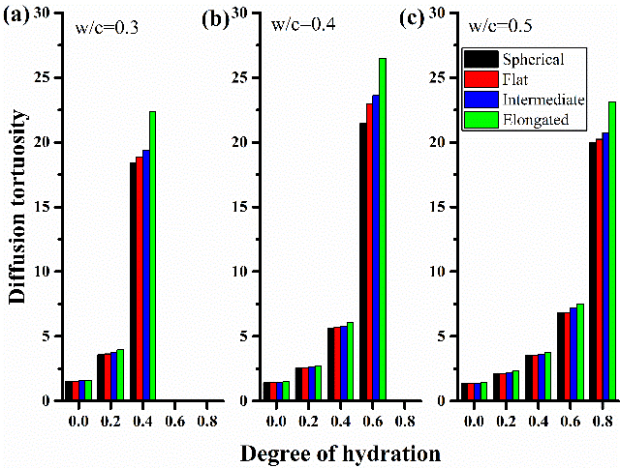

Fig. 15. Diffusion tortuosity in hardened cement pastes against degree of hydration.

It can be found that only the cement pastes consisting of extremely less equiaxed particles, e.g., elongated-shaped particles, show considerable difference of pore tortuosity at the same DoH. However, shapes of cement powders in the real cement particles do not show extremely non-equiaxed attributes. Ref. (Holzer *et al*., 2010) demonstrates that the average normalized length-to-width ratio is only between 1.27 and 1.46 for real cement particles. Herein, the length is defined as the largest-line surface point-to-surface point distance on the cement particle. The definition of width is satisfied with the largest-line surface point-to-surface point distance on the cement particle and the direction is perpendicular to the length as well. In terms of the numerical relationship between the normalized length-to-width ratio and principal moment of inertia of the particle used in this study, the square of normalized length-to-width ratio is approximately equal to the ratio of the maximum principal moment of inertia to the minimum principal moment of inertia (Holzer *et al*., 2010). After deduction, the average degree of irregularity of real cement particles is similar to the simulated intermediate-shaped particles with the average normalized length-to-width ratio of 1.41, but much smaller than elongated-shaped particles with the ratio of 2.08. Consequently, it can be concluded that particle shaped geometry of cement particles has slight effect on pore tortuosity in hardened cement pastes.

4.0 CONCLUSIONS

In this paper, the effects of cement particle shapes on capillary pore structures in hardened cement pastes are investigated in detail, which is simulated using a discrete-based hydration model. Some algorithms along with home-made programs for determining 3D pore structure parameters including porosity, pore size distribution, pore connectivity and pore tortuosity, are carried out on the simulated cement pastes consisting of different particles with representative irregular shapes. Based on the findings of this study, the following conclusions can be drawn:

(1) Cement particle shapes have considerable effects on pore structure parameters in cement pastes at the early curing age, while this effect will decrease as time elapses. Due to high area surface, the less equiaxed cement particles can contribute to cement hydration, which leads to corresponding hardened cement pastes with less porosity, smaller pore size, faster pore depercolation and more tortuosity in the early curing period, compared to equiaxed ones. Meanwhile, large water-to-cement ratio is beneficial to extending this effect resulting from surface area difference of cement particles to some degree.

(2) Besides the dramatic influence factor, surface area of cement particles, the less considered geometric attribute of irregular shaped particle also plays a slight role in pore structure parameters in cement pastes. The less equiaxed particle is positive to decreasing pore size, accelerating capillary pore depercolation process and increasing pore tortuosity. However, the geometric attribute of cement particles generally shows a weak influence on the evolution of pore structures in cement pastes overall.

Acknowledgement

The financial support from National Natural Science Foundation of China (No. 51378116, No. 51678143 and NO. 51408597), Ministry of Science and Technology of China (973 Program, No. 2015CB655102) and China Scholarship Council (CSC) are gratefully acknowledged. The authors also would like to thank Dr. Dale Bentz from the National Institute for Standards and Testing, USA, for kindly providing the source codes of CEMHYD3D model.

References

Abyaneh, S.D., Wong, H., Buenfeld, N., 2013. Modelling the diffusivity of mortar and concrete using a three-dimensional mesostructure with several aggregate shapes. Computational Materials Science, 78: 63-73.

Bentz, D.P., 1995. A three-dimensional cement hydration and microstructure program: I. hydration rate, heat of hydration, and chemical shrinkage. Building and Fire Research Laboratory, National Institute of Technology.

Bentz, D.P., 1997. Three‐Dimensional Computer Simulation of Portland Cement Hydration and Microstructure Development. Journal of the American Ceramic Society, 80(1): 3-21.

Bentz, D.P., Garboczi, E.J., 1991. Percolation of phases in a three-dimensional cement paste microstructural model. Cement and Concrete Research, 21(2-3): 325-344.

Bullard, J.W., Garboczi, E.J., 2006. A model investigation of the influence of particle shape on portland cement hydration. Cement and Concrete Research, 36(6): 1007-1015.

Chindaprasirt, P., Jaturapitakkul, C., Sinsiri, T., 2005. Effect of fly ash fineness on compressive strength and pore size of blended cement paste. Cement and Concrete Composites, 27(4): 425-428.

Chindaprasirt, P., Jaturapitakkul, C., Sinsiri, T., 2007. Effect of fly ash fineness on microstructure of blended cement paste. Construction and Building Materials, 21(7): 1534-1541.

Dong, H., Gao, P., Ye, G., 2017. Characterization and comparison of capillary pore structures of digital cement pastes. Materials and Structures, 50(2): 154.

Gao, Y. *et al*., 2013. Characterization of ITZ in ternary blended cementitious composites: experiment and simulation. Construction and building Materials, 41: 742-750.

Garboczi, E., Bentz, D., 1992. Computer simulation of the diffusivity of cement-based materials. Journal of materials science, 27(8): 2083-2092.

Holzer, L., Flatt, R.J., Erdoğan, S.T., Bullard, J.W., Garboczi, E.J., 2010. Shape comparison between 0.4–2.0 and 20–60 μm cement particles. Journal of the American Ceramic Society, 93(6): 1626-1633.

Huang, Q., Jiang, Z., Gu, X., Zhang, W., Guo, B., 2015. Numerical simulation of moisture transport in concrete based on a pore size distribution model. Cement and Concrete Research, 67: 31-43.

Ishizaki, K., Komarneni, S., Nanko, M., 2013. Porous Materials: Process technology and applications, 4. Springer Science and Business Media.

Kuo, W.-Y., Huang, J.-S., Lin, C.-H., 2006. Effects of organo-modified montmorillonite on strengths and permeability of cement mortars. Cement and Concrete Research, 36(5): 886-895.

Liu, C., Huang, R., Zhang, Y., Liu, Z., Zhang, M., 2018a. Modelling of irregular-shaped cement particles and microstructural development of Portland cement. Construction and Building Materials, 168: 362-378.

Liu, C. *et al*., 2018b. Numerical simulation of the effect of cement particle shapes on capillary pore structures in hardened cement pastes. Construction and Building Materials (under revision).

Liu, Z., Chen, W., Zhang, Y., Lv, H., 2016. A three-dimensional multi-scale method to simulate the ion transport behavior of cement-based materials. Construction and Building Materials, 120: 494-503.

Mindess, S., Young, J.F., Darwin, D., 2003. Concrete. Prentice Hall.

Promentilla, M.A.B., Cortez, S.M., Papel, R.A.D., Tablada, B.M., Sugiyama, T., 2016. Evaluation of microstructure and transport properties of deteriorated cementitious materials from their X-ray computed tomography (CT) images. Materials, 9(5): 388.

Promentilla, M.A.B., Sugiyama, T., Hitomi, T., Takeda, N., 2009. Quantification of tortuosity in hardened cement pastes using synchrotron-based X-ray computed microtomography. Cement and Concrete Research, 39(6): 548-557.

Tsivilis, S. *et al*., 1999. The effect of clinker and limestone quality on the gas permeability, water absorption and pore structure of limestone cement concrete. Cement and Concrete Composites, 21(2): 139-146.

Xu, W., Chen, H., 2012. Microstructural characterization of fresh cement paste via random packing of ellipsoidal cement particles. Materials Characterization, 66: 16-23.

Zhang, Y., Liu, C., Liu, Z., Liu, G., Yang, L., 2017. Modelling of diffusion behavior of ions in low-density and high-density calcium silicate hydrate. Construction and Building Materials, 155: 965-980.